Chapter 3

The shape of the luminosity profiles of bulges[†]

Using a 2D generalization of Kent's model-independent decomposition method, we extract the K-band light profiles of the bulges of a sample of field galaxies with morphological types ranging from S0 to Sbc. We then examine the shape of the bulge profiles, by means of fitting a seeing-convolved power law of the form $\mu(r) \propto r^{1/n}$, where the exponent n is allowed to vary. The best-fitting exponent n is found to vary systematically from values around 1 (exponential) to 6 from late- to early-type bulges; the profiles tend to fall off more steeply in the outer parts for the later types. The same trend is seen as a function of bulge to disk ratio. Application of the method to artificial data proves that this result is not caused by disk-light contamination. There are also indications that n becomes larger with increasing total luminosity and radius of the bulge. A similar relation has recently been found for elliptical galaxies. The smooth trend of n with morphological type shows that the formation of or interaction with the disk has affected the density distribution of the bulge.

1 Introduction

Many unsolved problems regarding the formation, age and structure of galactic bulges have surfaced in the last few years. Due to the importance of these issues for our understanding of galaxy formation and evolution, photometric and kinematical modeling started to move away from the standards. The long-overdue questioning of the universality of the $r^{1/4}$ law (de Vaucouleurs 1948) as a means of describing the light profile came first for elliptical galaxies as systematic deviations began to appear (Michard 1985; Schombert 1986; van den Bergh 1989; Binggeli & Cameron 1991). Alternative descriptions of the bulges soon followed, and exponential forms were proposed as more suitable for the bulges of late-type spirals (Kent, Dame & Fazio 1991; Andredakis & Sanders 1994). Exponentials, however, are clearly not correct for the earlier types. Since some bulges are fitted well by the $r^{1/4}$ law, and others clearly better by an exponential, a functional form that is to fit the bulges in

[†]Y.C. Andredakis, R.F. Peletier & M. Balcells, Mon. Not. R. Astron. Soc. **275**, 874-888 (1995)

general needs an extra variable. The concept of the $r^{1/n}$ law was initially introduced by Sersic (1968). It was revived by Capaccioli (1988), who proposed the use of an $r^{2/9}$ law as an alternative for the description of the light profiles of ellipticals. The first full-scale implementation of this generalized de Vaucouleurs law was done by Caon, Capaccioli & D'Onofrio (1993). They used it to fit the major and minor axis profiles of a sample of ellipticals and S0s. The profiles spanned a large range of values in n, and it was found that n correlates with the effective radius and the total luminosity, in the sense that it becomes bigger (i.e. the profiles are shallower in the outer parts) for larger and brighter galaxies.

In this paper we examine the light profile shapes of a sample of spiral galaxies using the $r^{1/n}$ law mentioned above. For this, we use an extension of the model-independent decomposition method introduced by Kent (1986) to extract the bulge profile. The study of the surface brightness profiles of the bulges in the optical suffers from extinction by dust in the disk. Edge-on galaxies are in this way especially difficult to study. We circumvent the problem by using near-infrared K-band data. At 2.2 μm the images of the bulge and disk are much more regular, so that separation of these two components is easier. The sample and the observations are briefly described in Section 2, and the method is outlined in Section 3. In Section 4 we show the results of fitting the profiles using the generalized de Vaucouleurs law. In Section 5 we examine the dependence of n on parameters such as effective radius, absolute magnitude and B/D ratio; we find that n becomes bigger for earlier types and large bulge to disk ratios. We discuss possible causes of these correlations. We also compare global parameters of the bulges such as effective radius, effective surface brightness and total luminosity with those of elliptical galaxies. Finally, we summarize our conclusions in Section 6.

2 Sample, observations and reduction

We study a complete, diameter-limited, optically selected sample of early- to intermediate-type spirals, selected from the UGC Catalogue (Nilson 1973); a detailed description of the selection method is given in Balcells & Peletier (1994). The initial sample consisted of 32 field galaxies with morphological types ranging from S0 (T=−3) to Sbc (T=4). The main morphological criteria for the selection were that the major axis diameter should be more than 2 arcmin, and the axial ratio in B larger than 1.56, corresponding to inclinations above 50°. This is necessary for the specific decomposition method that we use, which requires that the apparent ellipticities of the bulge and disk are as distinct as possible. Since their purpose was to study stellar populations and colour gradients, Balcells & Peletier (1994) rejected galaxies that are very dusty, have a very small bulge or whose disk scalelength is strongly filter-dependent. For our purpose here we relax all of these criteria and analyse all the galaxies in their table 1 except UGC 8722 and 10851 which are too far north to be observed with UKIRT. The 12 galaxies that did not make it into the sample of Balcells & Peletier (1994) because they were too dusty all the way to the centre or belonged to an interacting system are also excluded from the sample of this paper. Thus we are left with 30 objects, whose UGC and NGC name, morphological type (from the RC3 Catalogue, de Vaucouleurs et al. 1991) and distance (H_0 = 75 km s^{-1}Mpc^{-1}) are listed in the first four

columns of Table 1.

The sample was observed in the J and K near-infrared passbands using the IRCAM3 camera on UKIRT at Mauna Kea. In our analysis we use the K frames, as at 2.2 μm the effects of dust extinction are minimized and the effective seeing is better. As an example, we give a B-band and a K-band image of the highly inclined UGC9428 in Fig. 1.

Although relatively large for an infrared camera, measuring 256×256 pixels with 0.286 arcsec per pixel, IRCAM3 is too small to contain these large galaxies. For each galaxy we observed a sequence of 10 frames: six frames of the galaxy, with the centre each time at a different place, and four of the neighbouring background sky. For reduction, a median-filtered sky frame was made of these four images. This frame was scaled and subtracted from each of the object frames. Following this the object frames were flat-fielded using a flat-field obtained from all dark sky frames of that night. Finally, a mosaic was made by combining the six frames, using the galaxy centre as the reference point, and adjusting the sky background of each frame individually. The final mosaics generally have a size of 120 × 100 arcsec and, since the galaxies are relatively close to edge-on, are large enough to determine and subtract the residual sky background on the frame. The seeing FWHM, as measured from bright stars on the images, ranges from 0.8 to 1.2 arcsec.

Following these reduction steps we calculate the surface brightness profiles and the total luminosities of the galaxies, by fitting elliptical isophotes to the images. The centre is kept fixed, but the ellipticity and the position angle are allowed to vary, in order to determine the ellipticity and position angle profiles that will be necessary later. The resulting major axis surface brightness profiles are given in Fig. 1, in Appendix A. The total absolute K magnitude of the galaxy is calculated by integrating inside the elliptical annuli, and is given in Table 1. Due to incomplete coverage, the magnitudes of some galaxies are slightly underestimated; these galaxies are indicated by an asterisk. Two barred galaxies in our sample are marked by a dagger. In columns 6 and 7 of Table 1 we give the ellipticities of the bulge and the disk for each galaxy; the way that these are determined is described in Section 3.3.

3 Bulge-disk Decomposition

3.1 Outline of the method

As mentioned earlier, an objective and model-independent bulge-disk decomposition method must be used, if we want to study the shape of the profile of one of these two components. It is also desirable to have model-independent estimates for the other photometric characteristics of the bulge such as effective (i.e. half-total light) radius, effective surface brightness and total magnitude. The classical decomposition methods, using an iterative or a simultaneous fitting of an exponential disk and an $r^{1/4}$ bulge (Kormendy 1977; Boroson 1981; Shaw & Gilmore 1989) make the a priori assumption that the bulge follows an $r^{1/4}$ law. This means that, after decomposition, deviations from this law cannot be studied. The only model-independent method that has been implemented until now is that of Kent (1986). The basic principle is that the bulge and the disk profiles are assumed to have,

Table 1: Morphological data.

UGC (1)	NGC (2)	Type (3)	Distance (4)	M_K^{abs} (5)	ϵ_{disk} (6)	ϵ_{bulge} (7)
8764	5326	1	51.5	-25.06	0.55	0.20
8835	5362	3	46.2	-23.63	0.63	0.33
8866	5389	0	39.3	-24.78	0.75	0.25
8935	5422	-2	38.0	-24.65	0.80	0.17
8958	5443	3	40.8	-24.43	0.72	0.27
9016	5475	1	36.8	-24.27	0.71	0.05
9187	5577	4	29.4	-22.02	0.72	0.30
9202	5587	0	46.5	-25.15	0.70	0.20
9357	5675	3	85.2	-25.78	0.68	0.10
9361	–	3	50.1	-25.20	0.75	0.40
9399	5689	0	45.5	-25.43	0.75	0.35
9428	5707	2	46.7	-24.74	0.75	0.15
9462	5719	2	34.6	-25.07	0.68	0.20
9499 ∗	5746	3	34.4	-25.84	0.83	0.27
9692 ∗	5838	-3	27.5	-24.60	0.63	0.10
9723	5866	-1	18.3	-24.68	0.64	0.10
9726	5854	-1	34.9	-24.42	0.70	0.20
9753	5879	4	20.7	-23.57	0.70	0.36
9805	5908	3	69.1	-27.04	0.81	0.30
9914	5965	3	71.4	-26.05	0.83	0.40
9971 ∗	5987	3	63.4	-25.96	0.65	0.25
10081	6010	0	39.0	-25.09	0.77	0.22
10856 †	6368	3	55.3	-25.19	0.67	0.15
11053	6504	2	92.8	-26.44	0.80	0.25
11401 †	6757	0	45.0	-24.16	0.54	0.10
12080	7311	2	90.7	-26.29	0.53	0.00
12115	7332	-2	29.3	-25.69	0.75	0.24
12306	7457	-3	20.5	-23.03	0.48	0.25
12442	7537	4	52.9	-24.44	0.66	0.20
12691 ∗	7711	-2	84.3	-25.75	0.75	0.20

Columns in Table 1: (1), (2) name of the galaxy; **(3)** morphological type from the RC3 Catalogue; **(4)** distance in Mpc, computed from the Galactic-standard-of-rest-corrected redshifts given in RC3 (H_0 = 75 km s^{-1}Mpc^{-1}); **(5)** absolute magnitude in the K band from our photometry; **(6)**, (7) ellipticities of the disk and the bulge.

in projection, elliptical isophotes of constant but different flattening. This difference in flattening is the key to the decomposition method; the major and minor axis profiles are

each the sum of the bulge and disk profiles, but each one of the latter is scaled radially by a different factor. This constitutes a system of two equations that can be solved iteratively to obtain the bulge or the disk profile. For illustrative purposes, we will give the equations here also: Let $B(r)$ and $D(r)$ be the (unknown) bulge and disk major axis profiles. Then, the intensities along the major and minor axis are, respectively,

$$I_{\rm maj}(r) = B(r) + D(r), \tag{1}$$

$$I_{\rm min}(r) = B(f_B r) + D(f_D r), \tag{2}$$

where f_D and f_B stand for the major to minor axial ratio of each component. Substituting $D(r)$ from equation (1) into equation (2) we have that

$$B(r) = W(r) + B(\lambda r) \tag{3}$$

where $W(r) = I_{\rm min}(r/f_B) - I_{\rm maj}(r f_D/f_B)$ and $\lambda = f_D/f_B$. We solve equation (3) iteratively, using the method of Kent (1986), as follows. In the first iteration we assume that $B(r)$ is equal to $W(r)$ and we substitute this into the right-hand side of equation (3), getting

$$B(r) = W(r) + W(\lambda r). \tag{4}$$

This process is repeated indefinitely, yielding

$$B(r) = W(r) + W(\lambda r) + W(\lambda^2 r) + W(\lambda^3 r) + ... \tag{5}$$

or, in condensed form,

$$B(r) = \sum_{k=0}^{\infty} W[(\frac{f_D}{f_B})^{k} r]. \tag{6}$$

Since $W(r)$ is a declining function of radius and λ is greater than 1, convergence of the series is guaranteed. A variance of this method was used by Capaccioli (1987), and a generalization using variable ellipticities was used by Simien & Michard (1990). The method is simple and robust, and can be extended in many ways. A built-in disadvantage is that it cannot cope with galaxies that are close to face-on (small difference in apparent flattenings), or with galaxies with significant isophote twisting. Another disadvantage is that the presence of features like spiral arms and dust lanes can cause spurious bumps or dips in the major and minor axis light distributions. If, on the other hand, raw cuts are used instead of elliptical isophotes, there are always features on the major axis that are not present on the minor axis, again causing abnormalities or even oscillations on the derived bulge and disk profiles.

To circumvent this last problem, we extended Kent's method to work on the raw two-dimensional light distribution. The principle is as follows. Let us consider two radial cuts of the image of the galaxy, from the centre outwards. Let the intensity along these two cuts be represented by two vectors, X and Y. Vector X forms an angle θ_1 with the major axis of the galaxy, and vector Y an angle θ_2, where $\theta_1 < \theta_2$. Then we can write down a pair of equations analogous to equations (1) and (2) above:

$$X(r, \theta_1) = B(b_1 r) + D(d_1 r), \tag{7}$$

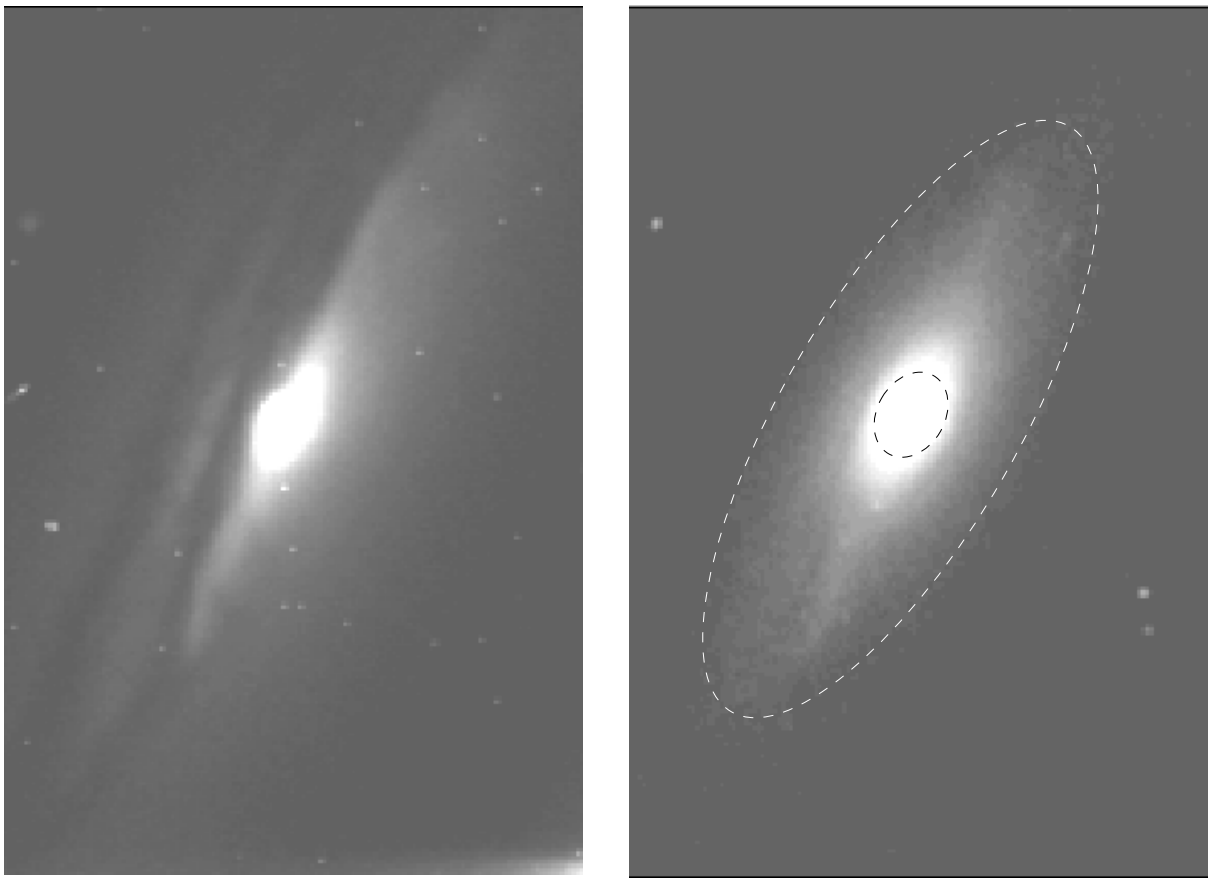

Figure 1: A B-band *(left panel)* and a K-band *(right panel)* image of UGC9428 shown side by side, to illustrate the great differences in terms of extinction. Note the much more regular appearance of both bulge and disk in the K image, mainly due to the absence of dust lanes. The adopted ellipticities of the bulge and the disk are drawn on the K-band image. For the ellipticity determination, see §3.3

$$Y(r,\theta_2) = B(b_2 r) + D(d_2 r). \tag{8}$$

The coefficients b_i and d_i depend on the azimuthal angle θ_i and the ellipticities of the bulge and the disk:

$$b_1 = \sqrt{\frac{1-(e_B\cos\theta_1)^2}{1-{e_B}^2}}, \qquad d_1 = \sqrt{\frac{1-(e_D\cos\theta_1)^2}{1-{e_D}^2}}, \tag{9}$$

$$b_2 = \sqrt{\frac{1-(e_B\cos\theta_2)^2}{1-{e_B}^2}}, \qquad d_2 = \sqrt{\frac{1-(e_D\cos\theta_2)^2}{1-{e_D}^2}}, \tag{10}$$

where e_i is the eccentricity of the corresponding component, $e = \sqrt{1-(b/a)^2}$. The solution of equations (5) and (6) for the *deprojected* (i.e. face-on) bulge profile $B(r)$ is

$$B(r) = \sum_{k=0}^{\infty} W[(\frac{d_2 b_1}{d_1 b_2})^{k} r] \tag{11}$$

where

$$W(r) = Y(\frac{r}{b_2}) - X(\frac{d_2 r}{b_2 d_1}) \tag{12}$$

The angle $\theta = (\theta_1 - \theta_2)$ between vectors X and Y should be such that any information about spiral arms, dust lanes and other ellipticity-scaled features is retained in both vectors, but at the same time large enough so that the profiles along X and Y are everywhere distinct. For the galaxies of our sample, without very prominent features, an angular difference of 35° to 45° is sufficient. Initially, vector X is placed on the major axis of the galaxy and vector Y is displaced by, say, 40° in the direction of the spiral arms, if they are present. The bulge profile is then determined by equation (11). Then, keeping the angle θ between them fixed, we move the vectors by 1°, and determine the bulge profile again. This procedure is repeated until the whole galaxy is covered. The vectors must always lie in the same quadrant of the galaxy, though, so that the 'effective' angle between them is always the same. In other words, if the vectors lie on either side of the major or the minor axis of the galaxy, then we are sampling two directions along which there is essentially no scaling difference. For this reason, when vector Y reaches the major or the minor axis, vector X changes to leading, instead of trailing behind Y. When the whole procedure is finished, the results of every angular step are averaged to give the final bulge profile. The standard deviation of the averaged points is then used as an uncertainty estimate, and the corresponding point of the final profile is weighted by this standard deviation in the fit that will follow.

In summary, we sweep the galaxy azimuthally by 360°, searching for features that are scaled by a certain ellipticity. The result is a very smooth, high signal-to-noise ratio bulge profile. The basic demands of the method are that the bulge and disk are as distinct as possible in ellipticity – i.e. we require galaxies with inclinations more than about 50°– and that there are no other features that can significantly affect the ellipticity, such as prominent bars, polar rings and warps.

3.2 Testing of the algorithm

We test the ability of our algorithm to distinguish and retrieve a bulge component of a certain ellipticity by applying it to artificial images of galaxies. A quick inspection of the major axis profiles of our galaxies shows that the outer parts are very well represented by an exponential disk, whose extrapolated central surface brightness lies close to 16 K mag arcsec^{-2}for most of the galaxies. The scalelength of the disk shows also a small scatter. Therefore we decided to model the disk using an exponential profile with central surface brightness and scalelength fixed to 16 K mag arcsec^{-2}and 25 arcsec respectively.

For the bulge, we have to use a more general form for the profile since we expect the late-type galaxies to have a bulge that is closer to exponential than to the traditional $r^{1/4}$ law (Kent et al. 1991; Andredakis & Sanders 1994; de Jong 1995). This required generic function was introduced by Sersic (1968) and has the form

$$\mu_B(r) \propto (r/r_0)^{1/n} \tag{13}$$

or, in intensity,

$$\Sigma(r) = B_0 \exp(-r/r_0)^{1/n} \quad (14)$$

where B_0 is the central surface brightness of the bulge, r_0 a general scaling factor, and n can take any positive value. Equations (13) and (14) describe a family of profiles, whose shapes depend on the value of n; as n becomes smaller, the profiles fall off more steeply at large radii. For $n = 1$ we have a simple exponential and for $n = 4$ the well-known de Vaucouleurs law.

In our artificial galaxies we vary all three of the bulge parameters (B_0, r_0 and n) in order to sample as big a range of bulge shapes and sizes as possible. (Keeping the disk fixed, this accounts also for the different B/D ratios.) The values of n that we use are 1, 2, 4, and 6. Then, for each of these values of n we use a number of different B_0s and r_0s. Since 27 out of our 30 galaxies have a B_0 that lies between 12 and 14 K mag arcsec^{-2}, we set the B_0 of the artificial galaxies to have these two values *after seeing convolution*. (This means that an $r^{1/4}$ law, for example, has to have a B_0 of 9.5 K mag arcsec^{-2}in order for B_0 to be 12 after seeing convolution.) The values for r_0 that we use are 10, 18 and 25 arcsec. Poisson noise is then added to the images, at a level comparable to that of the real data, and finally the images are convolved with a Gaussian kernel to mimic the seeing effects. The whole procedure is repeated for three different disk ellipticities: 0.60, 0.75 and 0.82, corresponding roughly to inclination angles of 67°, 77°and 85° respectively. The ellipticity of the bulge is kept fixed to the fairly representative value of 0.2; as will be shown in the next section, the decomposition results are not very sensitive to the ellipticity of the bulge within the expected values (0.0 to 0.4). In Fig. 2 we show the input and output profiles for $n = 1, 2$ and 4, and for both bulge B_0.

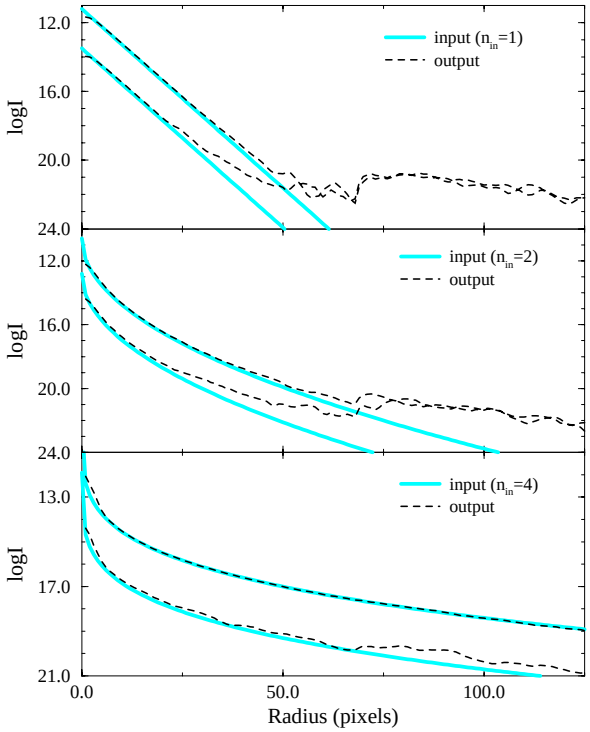

Figure 2: Input unconvolved artificial bulge profiles (thick grey lines) and output from the decomposition algorithm (dashed lines). For the n-values of the output profiles, see Table 2.

After applying our algorithm to these artificial images, we fit the resulting profiles using the seeing-convolved form of equation (14):

$$\Sigma_c(r) = \sigma^{-2} \exp(-r^2/2\sigma^2) \int_0^\infty \Sigma(x) I_0(xr/\sigma^2) \times \exp(-x^2/2\sigma^2) x \mathrm{d}x. \quad (15)$$

In equation (15) σ is the sigma of the point-spread function and I_0 the zeroth-order modified Bessel function. The free parameters of the fit are B_0, r_0 and n. From the results of the fitting, we draw the following conclusions.

(1) The ability of the algorithm to detect and retrieve the bulge of a galaxy depends only very weakly on the inclination angle of the galaxy and on the radial scale (r_0) of the bulge, within the range of values that we used for these parameters. In general the results are slightly better for higher inclinations and larger sizes. In what follows, we fix the ellipticity of the disk to 0.75, and the r_0 of the bulge to 10 arcsec, a value that is fairly typical for a real bulge.

Table 2: Simulations on artificial galaxies.

n_{input}	B_0	cutoff	n_{output}
1	12.0	18.0	1.01
		19.0	1.05
		21.0	1.18
	14.0	18.0	1.02
		19.0	1.31
		21.0	1.94
2	12.0	18.0	1.83
		19.0	1.98
		21.0	2.41
	14.0	18.0	1.83
		19.0	2.08
		21.0	2.64
4	12.0	18.0	3.93
		19.0	3.94
		21.0	3.94
	14.0	18.0	3.95
		19.0	4.03
		21.0	4.11
6	12.0	18.0	5.62
		19.0	5.75
		21.0	5.75
	14.0	18.0	5.93
		19.0	5.96
		21.0	5.96

(2) Depending on the value of n, the algorithm reproduces excellently the shape and the other parameters of the bulge, within a certain range of surface brightness. For the larger values of n , in other words for profiles close to the $r^{1/4}$ law or even shallower, the output profile is practically indistinguishable from the original one throughout the whole radial range. For the smaller values of n ($r^{1/2}$ law and exponential), the original profile is again reproduced very accurately until a certain point; after that it begins to flatten off, while the original profile continues dropping. This effect is easy to understand. The

bulges with higher n fall off much more slowly, and they give a detectable (i.e. higher than the noise level) contribution even at large radii. The steeper bulges drop below the noise level relatively soon, and the algorithm from there on detects only the background noise. This, in combination with the disk light, produces a constant or slightly declining low-level signal that is output also as 'bulge'. The point at which this artificial flattening begins depends on the central surface brightness (c.s.b.) of the bulge, or, in other words, on the prominence of the bulge relative to the disk. For $B_0 = 12$ K mag arcsec^{-2}, where the bulge is 4 mag brighter than the disk in the centre, the output profile begins to differ from the input profile at around 19 K mag arcsec^{-2}for the case of $n = 1$. For $B_0 = 14$ K mag arcsec^{-2}, though, this departure begins already at 18 K mag arcsec^{-2}, and use of points beyond this limit would cause the n of the output profile to jump suddenly to very high values. In Table 2 we give a summary of these results in the form of output n as a function of input n, B_0 and cutoff magnitude. In general we can say that, if the results are biased, this bias is one sided. A relatively faint low-n bulge would look like a high-n one if we took into account data points beyond a certain surface brightness limit. A high-n bulge, on the other hand, will always be reproduced as such, irrespective of the range of points used. For conciseness, though, in the following analysis of the real data we will use a limit of 18.5 K mag arcsec^{-2}for all the bulges. For three galaxies in which the c.s.b. of the bulge is only two magnitudes higher than that of the disk, namely UGC 9723, 9805 and 9914, we restrict the limit to 17.5, in accordance with the above results.

3.3 Assumptions and errors of the method

The key parameters in the whole procedure are the ellipticity of the bulge and the disk, and the basic assumption is that these two components can be adequately described by elliptical isophotes with constant ellipticity, and common centre and position angle. For disks that are non-warped this is a fairly good approximation. For the bulge, this assumption requires that its intrinsic shape be that of an oblate spheroid, and this has to be justified. For our bulges, we find that generally the position angle outside the inner 3 arcsec is fairly constant. There is occasionally some evidence for isophote twisting within the inner 10 arcsec, but it does not exceed 2° in amplitude. There are two exceptions to this rule, UGC 9428 and UGC 9692, with a twisting amplitude in the inner 12 arcsec of around 15°. These two galaxies appear to have genuine triaxial bulges, since there are no spiral arms or dust lanes that could explain the isophote twisting. Apart from these, the rest of the bulges are consistent with being oblate. More important for the resulting shape of the surface brightness profile is the choice

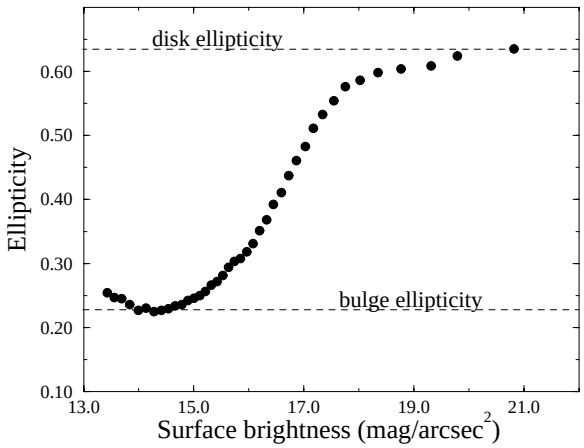

Figure 3: Typical run of ellipticity as a function of radius. The two relatively constant regions are taken to represent the bulge and disk ellipticities.

of bulge and disk ellipticities. A related question is whether we should use a constant or a variable ellipticity for the bulge. The problem with allowing the bulge ellipticity to vary is that it gets very difficult to separate variations in bulge ellipticity from those in disk ellipticity, and the definition of bulge and disk starts getting ambiguous. For this reason the bulge ellipticity is kept constant. The way that this ellipticity is determined is shown in

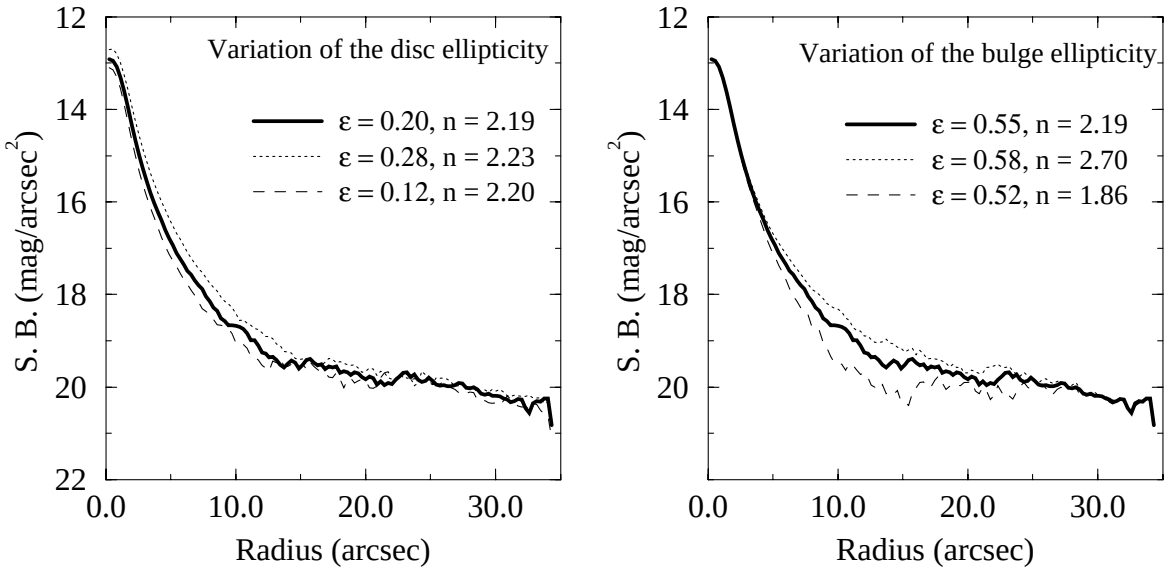

Figure 4: The effects of varying the disk and bulge ellipticities by their corresponding uncertainties in the bulge profile of UGC 8764. The best-fitting n of the $r^{1/n}$ law is also given for each case.

Fig. 3, where we plot the ellipticity of a galaxy's isophotes as a function of surface brightness. In such a plot it is easy to make out two regions in which the ellipticity remains practically constant; these two values are adopted as the ellipticities of the bulge and the disk. Using this method, the bulge ellipticity close to the centre is usually overestimated, and too much light is attributed to the bulge there. As a result, the disk profile usually has a non-physical 'hole' of negative values in the central 2 or 3 arcsec. The effect that this has on the bulge profile, however, is very small, since in these regions the bulge is two or more magnitudes brighter than the disk. When the ellipticity profile does not show these two flat regions, but rises rapidly from the centre towards an asymptotic value, we adopt the minimum value as the bulge ellipticity.

In general, the ellipticity of the bulge is not easy to determine by any method, and errors of the order of 30 per cent are possible. Moreover, ellipse fitting to our artificial data shows that in general the ellipticity of the bulge will always be overestimated. Fortunately, it turns out that the shape of the resulting bulge profile is relatively insensitive to the adopted value for the ellipticity of the bulge. It is, however, very sensitive to the ellipticity of the disk which, in contrast, is very well constrained by the data for our inclined galaxies; it can be determined with an accuracy of 5 per cent or better. In Fig. 4 we show the effects of varying the adopted ellipticities of the bulge and the disk by their corresponding uncertainties on the bulge profile of UGC 8764. Fitting the profiles using formula (15),

we find that in the case of the bulge ellipticity the change in n is negligible, while for the disk ellipticity the change is rather significant. In particular, the underestimation of the disk ellipticity produces drastic effects; this underestimation is easily detectable visually, though, by the spurious flat-bottomed dip that it causes in the middle regions of the bulge profile.

Finally, we examine the effects of the sky subtraction on the resulting bulge profile (by 'sky' we mean here the residual background that is subtracted from the image as a constant, after the primary subtraction of sky frames). Especially in the K-band images this is important, since the sky level changes on rather short time-scales and this can result in uneven mosaicing, i.e. a non-uniform sky across the image. On our images there are not any significant residual gradients, but an over- or underestimation of the sky level is still possible. In Fig. 5 we plot the bulge profile of UGC 8764 with the adopted sky level increased and decreased by 5 and 10 counts. Expressed in magnitudes, this corresponds to a change of roughly 0.2 and 0.4 K mag arcsec^{-2}above and below the adopted 18.84 K mag arcsec^{-2}(this is the remaining sky after the first-order sky subtraction). An error of 10 counts is somewhat larger than the largest anticipated error in the sky value. It is easy to see that above the cutoff limit of 18.5 K mag arcsec^{-2}the change in the profile shape is small; the corresponding values of n are given in the figure. Concluding, we can say that the uncertainties in the disk ellipticity and in the sky subtraction are the main sources of error in the resulting bulge surface brightness profile. Quantitative estimates for these are made for each galaxy separately, and will be given in the next section.

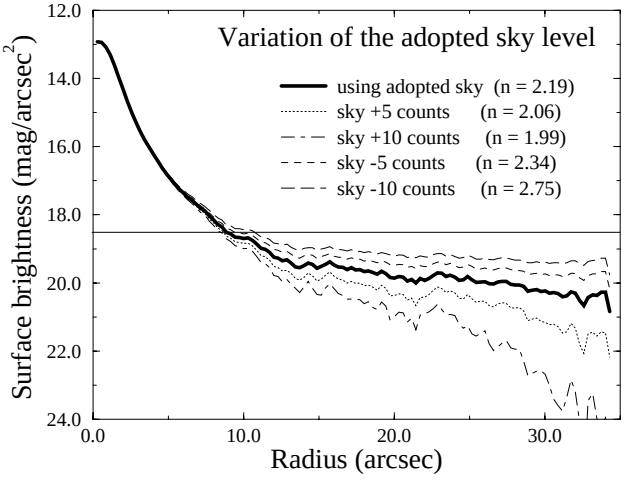

Figure 5: The effects of varying the adopted sky level in the bulge profile of UGC 8764.

4 The shape of the bulge profiles

Applying the decomposition algorithm to our images, we obtain the bulge profiles shown in Fig. A1. The profiles are in general well behaved, and decline monotonically until the surface brightness is too low to be distinguished from the background noise. From that point on, at a surface brightness level around 19.5–20 mag/arcsec^2, the output is a sum of noise plus a very small contribution from the disk. The two barred galaxies are the only ones that present abnormalities in their bulges profiles: UGC 11401, with a bar aligned with the disk, has a large hole in the middle parts of its bulge profile, while UGC 10856 shows a prominent bump. Another profile worth mentioning is that of UGC 9499. This very large galaxy (7 arcmin in diameter) is covered only as far as about one disk scalelength, with a surface brightness at the edge of the image as high as 16.5 K mag arcsec^{-2}. A simulation of

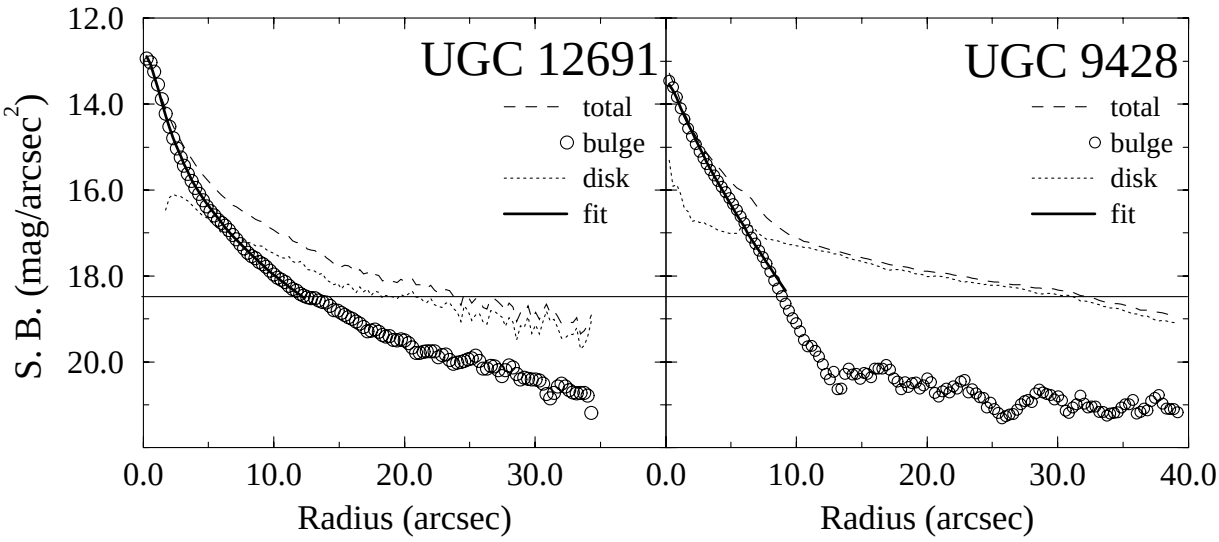

Figure 6: The bulge profiles and the fits of the $r^{1/n}$ law of UGC 12691 and UGC 9428. Also shown are the total surface brightness profiles and the disk profiles (subtraction of the bulge profile from the total). The solid line indicates the surface brightness cutoff used for the fit.

the limited coverage of this galaxy showed that our decomposition would give an extended shallow profile of the kind shown in Fig. A1 for the bulge, even with an input n of 1.0 (exponential bulge). For this reason, we exclude this galaxy from the subsequent statistics. The results of fitting the bulges using formula (15) are given in Table 3. In columns (2) to (6) we give the surface brightness cutoff for each galaxy, the corresponding radius (i.e. $R_{18.5}$), the absolute magnitude inside the cutoff radius ($M_{18.5}$), the best-fitting power n and its total error. In columns (7) to (11) we give the effective radius ($R_{\rm eff}$), the mean surface brightness inside $R_{\rm eff}$, the total absolute magnitude of the bulge, the bulge to disk ratio and finally the reduced χ^2 of the fit. The parameters in columns (7) to (10) are determined by integrating the actual profile until the cutoff, and then integrating an extrapolation of the best-fitting $r^{1/n}$ law from the cutoff to the last measured point. This is necessary, if we want to have realistic estimates of parameters referring to the whole bulge. For the correlations with n, though, we use the radius and luminosity of the bulge inside the cutoff (i.e. $R_{18.5}$and $M_{18.5}$), which are completely independent of n.

The disk profiles shown in Fig. A1 are determined simply by subtracting the bulge profile from the total major axis profile. In most cases they are very well represented by exponentials except in the inner 1.5–2 arcsec; some disk profiles display a sudden dip to zero there. This is due to the ellipticity attributed to the bulge (see Section 3.3) and does not affect the bulge profile at all. The disk magnitude used in the B/D ratio is determined by straightforward integration of the profile until the last measured point.

The quoted error in n is estimated by varying independently the level of the sky that we subtract and the ellipticity of the disk by their corresponding uncertainties for each image, and then repeating the decomposition and fitting. The difference in the derived values of n gives an estimate of the corresponding contribution in the error. The total error is then the quadratic sum of these two contributions. We also tried to get an estimate of the

error introduced by including more data points, by shifting the cutoff magnitude to 19.0. The resulting change in the value of n is as a rule much smaller than the previous ones; the same goes for the typical uncertainty in n given by the fitting program. In the few cases where the last two uncertainties are significant, they are added quadratically to the total error. The results of changing the cutoff magnitude are also given in Table 2. As a highlight of the fitting results, we give the bulge and disk profiles of UGC 9428 ($T = 2$) and UGC 12691 ($T = -2$) that resulted from the decomposition in Fig. 6. We show the fit to the bulge profile, and we also indicate the surface brightness cutoff. We can see that the isophote twisting in UGC 9428 does not cause any observable abnormalities in the bulge profile. The reason for showing the results for these two galaxies separately is that they have identical disk ellipticities. Consequently, and taking into account the results in Section 3.2, the striking difference in shape between these two profiles cannot be attributed to the decomposition method or to the values of its parameters. It has to be real; the different morphological types of the two galaxies already give a hint to the cause of the difference.

The quality of the fits is in general very good. The residuals, if any, are statistical fluctuations of very low amplitude. As noted also in Caon et al. (1993) the $r^{1/n}$ law gives by definition better fits to the light profiles than any fixed power law like an $r^{1/4}$ law or an exponential. Its use is justified not by the improvement of the fits, but by the study of the values attained by n, and the possible correlations that n can have with the other parameters.

5 Discussion

5.1 Correlations of n with the bulge parameters

Immediately obvious from the results of Table 3 is the large spread of values of n. It ranges from 0.8, i.e. even steeper than an exponential law, to 6.2, i.e. much shallower than the $r^{1/4}$ law. Bulges of spirals display a rich diversity as far as the shape of the light profile is concerned, much in the same way as has been found for dwarf and for normal ellipticals, in the studies of Binggeli & Cameron (1991) and Caon et al. (1993) respectively. (It should be noted, though, that the highest value of n that we find for bulges is much lower than that of Caon et al., who find values up to $n = 17$ for giant ellipticals). This diversity also shows that use of a single law – like a de Vaucouleurs law or an exponential – to describe all the bulges is unrealistic, and can lead to serious under- or overestimations of the physical parameters of the bulge and the disk. The cause of this diversity can be either the influence of the other components of spirals, such as the disk and the halo, or an intrinsic feature of this family of objects, which has to do with formation processes. Discrimination between these two is difficult. We can get some idea, though, by searching for any systematic trends in this variety of profile shapes.

In Fig. 7(a),(b) and 8(a),(b) we plot n on a logarithmic scale versus the morphological type of the galaxy, the bulge to disk ratio, $M_{18.5}$and Reigh. In order to increase the range of morphological types in our sample, we performed the simple major and minor axis

Table 3: Results of fitting the $r^{1/n}$ law.

UGC (1)	cutoff (2)	$R_{18.5}$ (3)	$M_{18.5}$ (4)	n (5)	Δn (6)	R_{eff} (7)	SB_{eff} (8)	M_{bulge} (9)	B/D (10)	χ^2 (11)
8764	18.50	2.14	-23.23	2.19	0.45	0.54	13.88	-23.33	0.25	0.38
8835	18.50	1.41	-20.83	1.98	0.39	1.45	17.74	-21.63	0.17	0.10
8866	18.50	2.46	-23.15	3.07	0.24	0.89	14.94	-23.38	0.35	0.11
8935	18.50	2.48	-23.18	3.07	0.20	0.83	14.78	-23.39	0.42	0.32
8958	18.50	1.98	-22.40	2.86	0.35	0.93	15.69	-22.72	0.24	0.09
9016	18.50	1.28	-21.84	2.52	0.25	0.46	14.83	-22.04	0.14	0.62
9187	18.50	0.74	-19.40	0.75	0.18	0.59	17.48	-19.92	0.16	0.01
9202	18.50	1.35	-21.70	1.53	0.21	0.48	15.13	-21.83	0.05	0.09
9357	18.50	3.54	-23.86	3.10	0.32	1.39	15.16	-24.12	0.26	0.21
9361	18.50	3.40	-24.23	2.28	0.31	0.82	13.80	-24.33	0.76	0.36
9399	18.50	4.99	-24.51	5.90	0.62	2.06	15.39	-24.75	0.93	0.21
9428	18.50	2.07	-23.19	1.30	0.27	0.77	14.71	-23.29	0.35	0.92
9462	18.50	1.92	-22.76	2.26	0.10	0.65	14.69	-22.93	0.16	0.03
9499	18.50	6.30	-24.91	4.10	0.43	2.43	15.57	-24.93	0.75	0.12
9692	18.50	3.78	-23.91	4.04	0.34	1.00	14.56	-24.01	1.24	0.10
9723	17.50	1.58	-22.08	3.98	0.91	0.60	15.04	-22.43	0.14	0.26
9726	18.50	2.08	-22.73	4.12	0.47	1.02	15.53	-23.08	0.37	0.46
9753	18.50	0.55	-19.45	2.21	0.31	0.23	15.68	-19.72	0.03	0.92
9805	17.50	3.10	-23.75	3.01	0.59	1.52	15.26	-24.22	0.08	0.53
9914	17.50	4.06	-24.56	3.29	0.26	2.85	15.77	-25.07	0.55	0.23
9971	18.50	2.55	-24.25	3.50	0.27	1.41	14.64	-24.67	0.39	0.07
10081	18.50	1.73	-23.00	2.21	0.34	0.46	13.76	-23.09	0.19	0.59
10856	18.50	3.15	-23.09	4.35	0.82	3.08	17.17	-23.84	0.34	0.11
11053	18.50	5.79	-24.89	2.59	0.36	2.24	15.21	-25.10	0.38	0.78
11401	18.50	1.25	-21.80	2.60	0.41	0.36	14.40	-21.92	0.14	0.16
12080	18.50	3.15	-24.26	1.32	0.12	0.87	13.95	-24.31	0.19	0.27
12115	18.50	2.36	-24.11	4.48	0.27	0.54	12.97	-24.24	0.35	0.20
12306	18.50	1.19	-21.19	6.24	1.44	0.85	16.50	-21.71	0.37	0.71
12442	18.50	0.88	-20.68	0.89	0.19	0.38	15.69	-20.80	0.04	0.04
12691	18.50	5.61	-24.83	3.27	0.28	2.06	15.07	-25.06	0.93	0.38

Columns in Table 3: **(1)** UGC number of the galaxy. **(2)** Cutoff magnitude for the fit. **(3)** Corresponding radius in kpc (for galaxies with a cutoff at 17.50, the $R_{18.5}$is determined by extrapolation). **(4)** Total absolute K–magnitude inside the cutoff. Same remark as for $R_{18.5}$. **(5)** The best-fitting exponent n of the $r^{1/n}$ law. **(6)** Total error in n . **(7)** Half-light (effective) radius of the extrapolated bulge profile in kpc. **(8)** Mean surface brightness inside R_{eff}. **(9)** Absolute K-magnitude (extrapolated) of the bulge. **(10)** Bulge to disk ratio. **(11)** The reduced χ^2 of the fit.

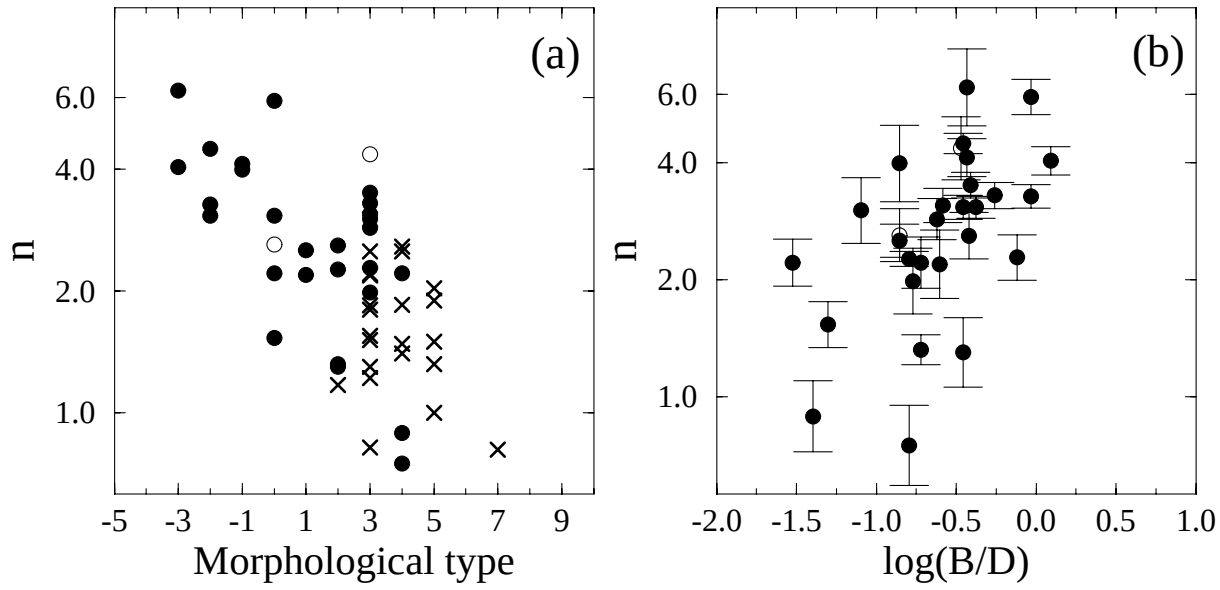

Figure 7: **(a)** The best-fitting n plotted (in logarithm) versus the morphological type of the galaxy. The galaxies of our sample are represented by the filled circles, the ones of Kent (1986) by crosses. The open circles indicate barred galaxies. No error bars are given in this plot, for clarity. **(b)** n versus bulge to disk ratio.

decomposition on the data of Kent (1986). His sample consists of 36 late type spirals, of which 23 are suitable for decomposition using this method. The resulting bulge profiles are then fitted using the same procedure as the galaxies of our sample. The results for these galaxies are given by different symbols (x). The two barred galaxies of our sample, UGC 10856 and 11401, are indicated by open circles.

Fig. 7(a) shows clearly that there is a good correlation of n with the morphological type of the galaxy. The mean value of n for the S0 galaxies of our sample ($T = -3$ to $T = 0$) is 3.7, with a standard deviation of 1.3. For types between T=1 and T=3 the mean value of n drops to 2.4 with an s.d. of 0.66, and for types between T=4 and T=7 n drops further down to 1.6 with an s.d. of 0.52. The scaling of the shape of the profile with morphological type is quite clear. The earlier types are close to the de Vaucouleurs law, although the scatter is large. This is more or less expected, given the morphological similarity between S0s and ellipticals and the success of the $r^{1/4}$ and the higher n laws in the description of the latter. The scatter should also be expected, since it is well known that S0 galaxies often suffer from misclassifications, present subclasses and are in general difficult to fit into a unified evolutionary scheme (van den Bergh 1994 and references therein). As we move towards the later types, the profiles become steeper, and are on the average described by an 'r to the half' ($r^{1/2}$) law. For Sc galaxies and later, the profiles are very close to pure exponentials. The significance of the correlation is more than 99.9 per cent, making this one of the strongest correlations found so far of a measurable parameter of a galaxy with its morphological type. Fig. 7b shows that the correlation of n with the B/D ratio is

almost as good as the one with the morphological type; this is natural, given that the (apparent) B/D ratio is usually the basic criterion for the classification of spirals. The linear correlation coefficient is 0.54 and the significance level is 99.7 per cent. These strong trends of n with type and B/D ratio are the main results of this paper. Although other possibilities cannot be excluded, the most straightforward explanation for this trend is that the presence of the disk affects the density distribution of the bulge in such a way as to make the bulge profile steeper in the outer parts. One mechanism to produce such an effect might be that a stronger disk truncates the bulge, forcing its profile to become exponential. As we will see, this suggestion could also be used to explain the correlations of n with the other parameters of the bulge, the absolute magnitude and the radius. For these two parameters we will use $M_{18.5}$ and $R_{18.5}$ as mentioned before.

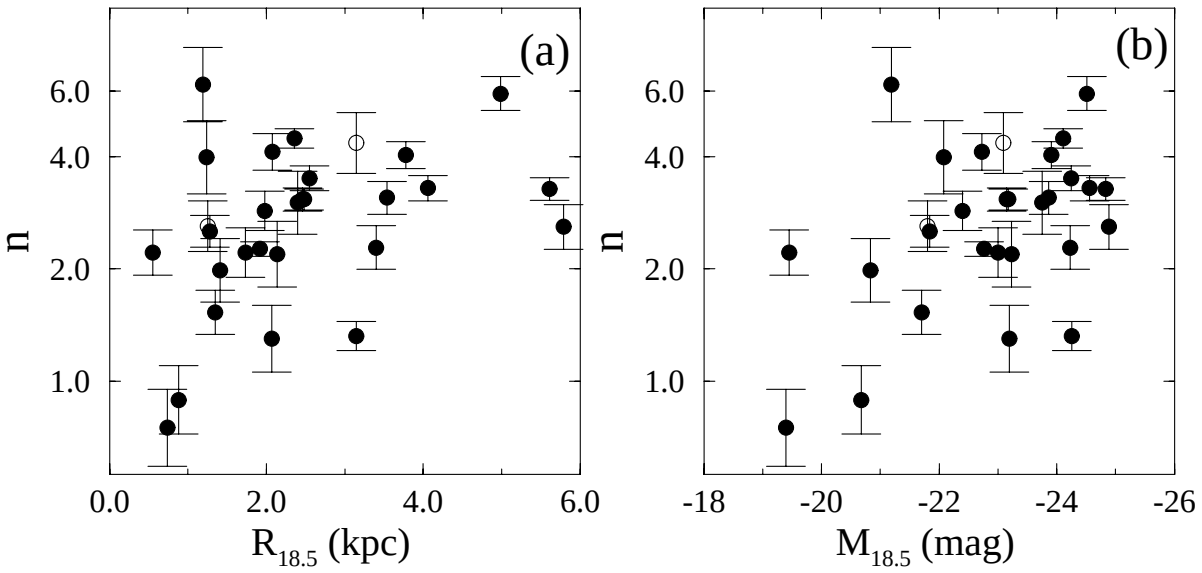

Figure 8: (a) The best-fitting n plotted versus $R_{18.5}$, taken to represent the radial extent of the bulge. **(b)** n plotted versus $M_{18.5}$, the integrated absolute magnitude of the bulge out to the last point used in the fit of the $r^{1/n}$ law. Both $M_{18.5}$and $R_{18.5}$are n-independent.

Fig. 8(a) shows that there exists a slight correlation between n and radius, in the sense that n becomes larger with increasing $R_{18.5}$. The scatter, though, is rather large; the linear correlation coefficient is equal to 0.38 at a significance level of 95.9 per cent. If we exclude the bulge of UGC 12306 which has the largest value of n as well as the highest uncertainty, the correlation becomes tighter, with a correlation coefficient $r = 0.47$. The trend is clearer in Fig. 8(b), showing how n correlates with the bulge absolute magnitude. Again excluding UGC 12306, we find a coefficient r of 0.54, at a significance level of 99.7 per cent. Although the scatter is large, we can conclude that n becomes larger with increasing total luminosity and effective radius; the larger and more luminous a bulge is, the shallower its profile at large radii. Caon et al. (1993) also found a trend of larger n with increasing $R_{\rm eff}$and absolute magnitude for their sample of ellipticals and S0s. Binggeli & Cameron (1991) found that the majority of dwarf ellipticals in the Virgo cluster are better described

by exponentials, i.e. n approaches 1 for these galaxies. Therefore, one more important similarity between bulges and ellipticals is revealed, just by dropping one of the traditional links between these two classes of objects: the description by an $r^{1/4}$ law. Bulges of spirals, being closer in luminosity to the intermediate and the dwarf ellipticals, are also described best by similar surface brightness laws. This comes in addition to the already known kinematical similarities, i.e. the fact that bulges are fast rotators, as well as low-luminosity ellipticals of high surface brightness; in contrast, the giant ellipticals do not rotate, and are supported mainly by velocity anisotropy (Franx 1992 and references therein). What causes this common behaviour?

There can be several possible explanations. There exists a common denominator, at least in bulges and normal ellipticals: the presence of a disk. It has been realized by now that most early-type galaxies have disks (Capaccioli, Caon and D'Onofrio 1992); the only truly diskless galaxies are the giant ellipticals at the centres of clusters. The relative size of the disk increases as we go from normal ellipticals to S0s, and then to early- and late-type spirals. This could give rise to a bigger disk – lower n sequence, in the sense that brighter ellipticals have relatively smaller disks and higher values of n than low-luminosity ellipticals, just as happens with early- and late-type spirals. However, the relative size of the disk does not vary smoothly with type for early-type galaxies. Disks in ellipticals are too small to have such an effect on the brightness profile of the spheroid. In addition, dwarf ellipticals have exponential profiles without any indications so far for having significant disks. So, it might well be that the observed scaling of n for ellipticals is an intrinsic property of these objects that depends only on parameters like the total mass or the size. This might be true even for bulges; the strong scaling of n with B/D ratio, though, cannot be ignored. A full exploration of the possible scenarios is beyond the scope of this paper; detailed theoretical modeling is required in order to proceed further in this problem.

Finally, there is one more interesting point about the scaling of n with morphological type. Pfenniger & Norman (1990) have proposed that many bulges are in fact inflated bars. It has also been argued (Kormendy 1992) that the bulges of later type spirals are in fact 'pseudo-bulges', formed by the accretion of disk material at the centre. If these late-type bulges were indeed formed by completely different mechanisms, we would not expect such a smooth scaling of n; a bi-modal distribution would be more logical. The continuity in the transition from $r^{1/4}$-like to exponential-like profiles that is actually observed fits better into a uniform rather than a bi-modal formation scenario for the bulges. An enrichment with disk material has undoubtedly taken place to some extent; this extent is probably larger for the lower B/D systems, and it might explain the observed differences in colours. The data tend to indicate, though, that all the bulges (with the possible exception of the peanut-shaped ones) formed by a common mechanism. Their surface brightness distribution was probably modified later, by the forces exerted by the stellar disk. We cannot claim that by this continuity in the profile shapes we can reject the picture of late-type bulges being formed by different mechanisms. One can probably devise a scenario in which bulge-like bars or pseudo-bulges can be affected by the disk or the halo in such a way as to create this shape-sequence. We do, however, offer an additional constraint in the whole picture that should be accounted for in the models of galaxy formation and evolution.

5.2 Bulges in the Fundamental Plane of elliptical galaxies

We have compared effective radii, effective surface brightness and absolute magnitudes of bulges with those from the large sample of early-type galaxies of Bender, Burstein & Faber (1992). To convert K-band luminosity and surface brightness to the B-band, used by Bender et al., we fit a least-squares relation to M_B as a function of $B-V$ for the sample of Bender et al. (1992). Then we use a relation between $B-V$ and $V-K$, derived from the aperture photometry of Persson, Frogel & Aaronson (1979) for all galaxies for which they have data in both bands. The final conversion formula used is

$$B-K \;=\; 1.477 - 0.1084\; M_K. \tag{16}$$

This conversion probably introduces an error of a few tenths of a magnitude per galaxy, but this is acceptable, when considering total magnitudes and surface brightness.

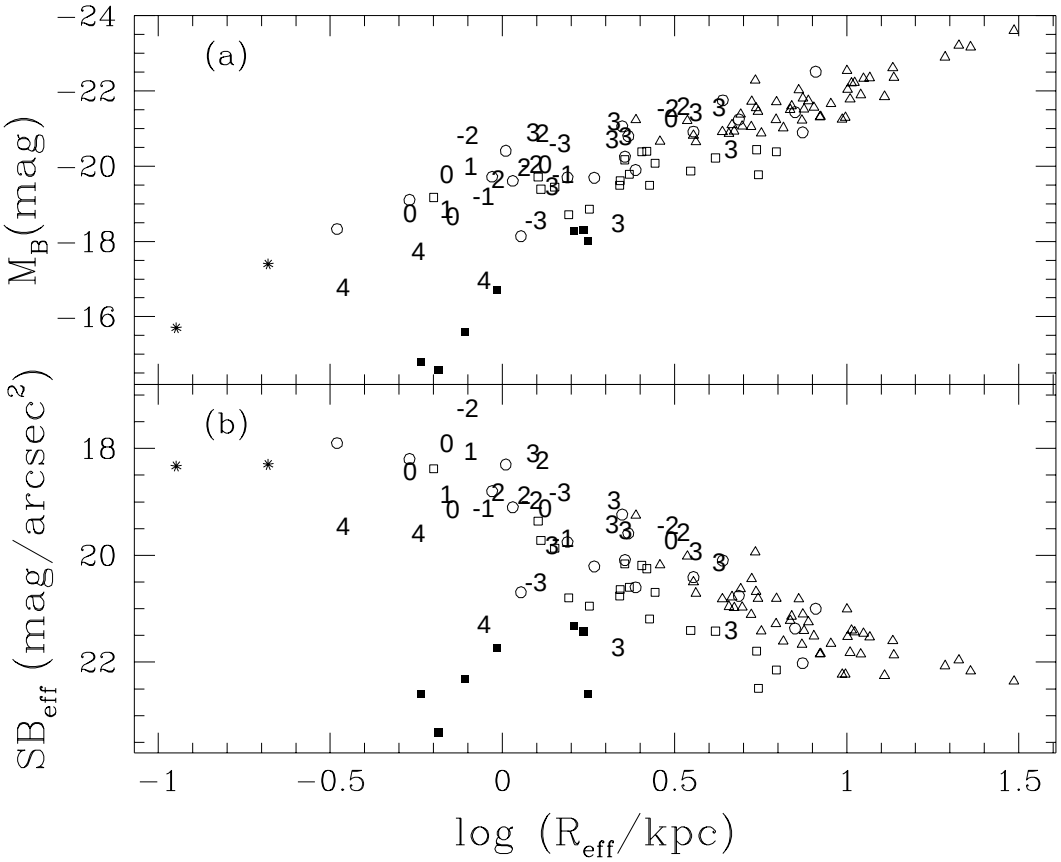

Figure 9: **(a)** The $R_{\rm eff}$– $M_{\rm abs}$ view of the Fundamental Plane. The bulges of our sample are given by the index T of their morphological type. All the other symbols represent the objects of Bender et al. (1992). Open triangles: normal ellipticals. Open squares: intermediate ellipticals. Asterisks: compact ellipticals. Filled squares: faint ellipticals. Open circles: bulges. The determination of $R_{\rm eff}$and $SB_{\rm eff}$ is explained in the text. **(b)** The $R_{\rm eff}$– $SB_{\rm eff}$ view of the Fundamental Plane. Symbols as in 7(a).

Fig. 9 shows the relations between effective radius, effective surface brightness within the effective radius, and absolute magnitude for all the objects. Bulges studied in this paper are indicated by numbers coding the galaxy type T (from Table 1). The various groups of galaxies from Bender et al. (1992) are indicated with different symbols, as given in the figure caption. Fig. 9(a) shows the relationship between effective radius and absolute magnitude. Most bulges in our sample fall in sequence with the rest of the bulges and ellipticals in the plot. Outliers with low surface brightness include all Sbc galaxies, one Sc and UGC 12306, an S0 with uncertain surface photometry. The rest of the points lie slightly below (about 1 mag) the distribution of points for the other objects, but define a similar slope. A least-squares fit to the data for our bulges, excluding the objects mentioned above, gives

$$M_B = -19.75 - 2.8 \log R_{\rm eff}. \tag{17}$$

Therefore, mean central (volume) density increases for lower luminosity bulges. Except for the outliers (three Sbc and one Sb), galaxy types are well mixed in this diagram. Therefore, the scaling of luminosity with effective radius appears to be largely independent of n, the shape of the surface brightness profile, given that n correlates well with type. The process which sets the observed scaling may well be independent from that which sets n.

Fig. 9(b) shows the relationship between effective radius and effective surface brightness. As is the case for Fig. 9(a), most bulges in our sample fall in sequence with the rest of the bulges and ellipticals. We find the same outliers as above. A least-squares fit to the data for our bulges, excluding the above-mentioned outliers, gives

$$SB_{\rm eff} = 18.80 + 2.25 \log R_{\rm eff}. \tag{18}$$

The galaxies that deviate most from the line of elliptical galaxies are predominantly low-luminosity bulges in late-type galaxies. Balcells & Peletier (1994) find that these deviant objects also deviate from the main colour–magnitude and from the colour gradient–magnitude relations of ellipticals and old bulges: they are bluer, and show steeper colour gradients. The deviations from the global parameter relations and from the colour–magnitude relation may indicate a discontinuity in the density–luminosity relation and in the stellar content along the Hubble sequence for types Sbc and later. This discontinuous transition argues against an environmental effect (the presence of a bigger disk in late types), and may be due to some specific feature of the formation of later type bulges. As noted above, no such discontinuity exists for the dependence of the shape parameter n on Hubble type: the steepening of the surface brightness profiles toward late types is progressive, and as such may be ascribed to an increasing effect of the disk. Whether bulges of Sbc and later types deviate from the Fundamental Plane of early-type galaxies remains to be seen, given the lack of velocity dispersions for our sample of bulges.

6 Conclusions

We introduce a two-dimensional extension of a bulge-disk decomposition method which uses the different ellipticities of these two components to extract the profile of the bulge.

We then apply this method to a sample of early-type spirals, complemented with literature data on later types. Our purpose is to study the shape of the luminosity distribution of the bulges of these galaxies and to examine the possible correlations that it can have with the global parameters of the bulge and of the galaxy as a whole. Our conclusions can be summarized as follows.

(1) The bulges of spiral galaxies show a remarkable diversity in the shapes of their light profiles. The parameter that describes the shape of the profile, the exponent n of the best-fitting power law, can have values that range from smaller than 1 (steep, close to exponential) to greater than 6 (shallower than the $r^{1/4}$ law). Therefore, the use of a single fitting law like a de Vaucouleurs law or an exponential is inadequate for the description of the bulge profiles in a sample of galaxies covering a wide range of morphological types.

(2) The shape of the bulge profile correlates well with the morphological type of the galaxy and with the bulge to disk ratio. Bulges of S0s are closer to an $r^{1/4}$ law, while bulges of late-type spirals are closer to exponential; there is a smooth transition between these two extremes. This suggests that the luminosity distribution of the bulge is affected by the presence of the disk in a systematic way: the larger the relative size of the disk, the steeper the bulge profile at large radii. The continuity in the spectrum of n might also imply that it is unlikely that the bulges of late type spirals were formed by a different mechanism from the ones of early types. Shape also correlates with the total luminosity of the bulge, in the sense that n is larger with increasing absolute magnitude. This is one more common characteristic between bulges and elliptical galaxies of comparable luminosity. It shows that, at least as far as the shape of the surface brightness profile is concerned, early-type bulges are more similar to elliptical galaxies than the late–type ones. Regarding global photometric parameters, bulges as late as Sb fall on the same $R_{\rm eff}$–M_B and $R_{\rm eff}$–$SB_{\rm eff}$ relations as ellipticals, whereas later types appear to depart systematically from these relations.

References

Andredakis, Y.C., Sanders R.H., 1994, MNRAS, 267, 283
Balcells M., Peletier R.F., 1994, AJ, 107, 135
Bender R., Burstein D., Faber S.M., 1992, ApJ, 399, 462
Binggeli B., Cameron L.M., 1991, A&A, 252, 27
Boroson T., 1981 ApJS, 46, 177
Caon N., Capaccioli M., D'Onofrio M., 1993, MNRAS, 265, 1013
Capaccioli M., 1987, in de Zeeuw P.T., ed., Proc. IAU Symp. 127, *Structure and Dynamics of elliptical Galaxies*. Reidel, Dordrecht p. 47
Capaccioli M., 1988, in H. Corwin, L. Bottinelli, eds, *The world of Galaxies*. Springer Verlag, Berlin p. 208
Capaccioli M., Caon N., D'Onofrio M., 1992, MNRAS, 259, 323
de Jong R.S., 1995, Ph.D. Thesis, Univ. of Groningen
de Vaucouleurs G., 1948, Ann. d'Astrophys., 11, 247
de Vaucouleurs G., de Vaucouleurs A., Corwin H. G., Buta R. J., Paturel G., Fouque P., 1991, Third Reference Catalogue of Galaxies. Springer Verlag, New York

Franx M., 1992, in Dejonghe H., Habing H., eds, Proc. IAU Symp. 153, *Galactic Bulges*. Kluwer, Dordrecht p. 243
Kent S.M., 1986, AJ, 93, 1301
Kent S. M., Dame T., Fazio G., 1991, ApJ, 378, 131
Kormendy J., 1977, ApJ, 217, 406
Kormendy J., 1992, in Dejonghe H., Habing H., eds, Proc. IAU Symp. 153, *Galactic Bulges*. Kluwer, Dordrecht p. 209
Michard R., 1985, A&A, 59, 205
Nilson P., 1973, *Uppsala General Catalogue of Galaxies*
Persson S.E., Frogel J.A., Aaronson M., 1979, ApJS, 39, 61
Pfenniger D., Norman C., 1990, ApJ, 363, 391
Schombert J.M., 1986, ApJ 60, 603
Sersic J.L., 1968, *Atlas de galaxias australes*. Observatorio Astronomico, Cordoba
Shaw M.A., Gilmore G., 1989, MNRAS, 237, 903
Simien F., Michard R., 1990, A&A, 227, 11
van den Bergh S., 1989, PASP, 101, 1072
van den Bergh S., 1994, AJ, 107, 153

A Plots of the bulge profiles

Here we give the bulge profiles that resulted from our decomposition, together with the total major axis profiles of the galaxies, the disk profiles (resulting from the subtraction of the bulge profile from the total) and the fits to the bulge profiles. The best-fitting n of the $r^{1/n}$ law is also given for each galaxy. The profiles are also available in tabular form from the authors.

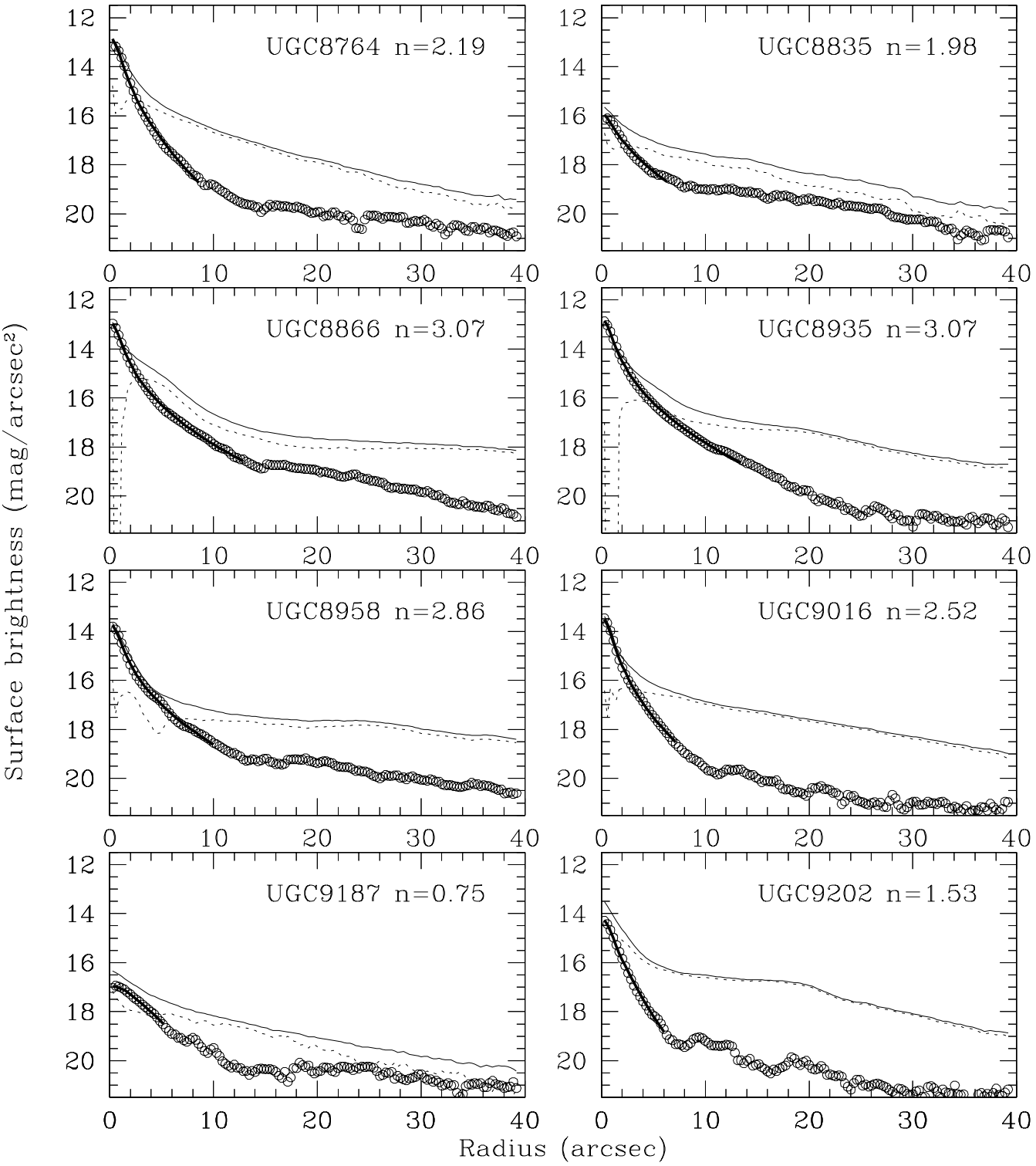

Figure 1: Plots of the results of the decomposition and fitting. The bulge profile is given by the open circles, the total profile by the thin solid line and the disk profile by the dotted line. The fit of the $r^{1/n}$ law to the bulge profile is given by the thick solid line.

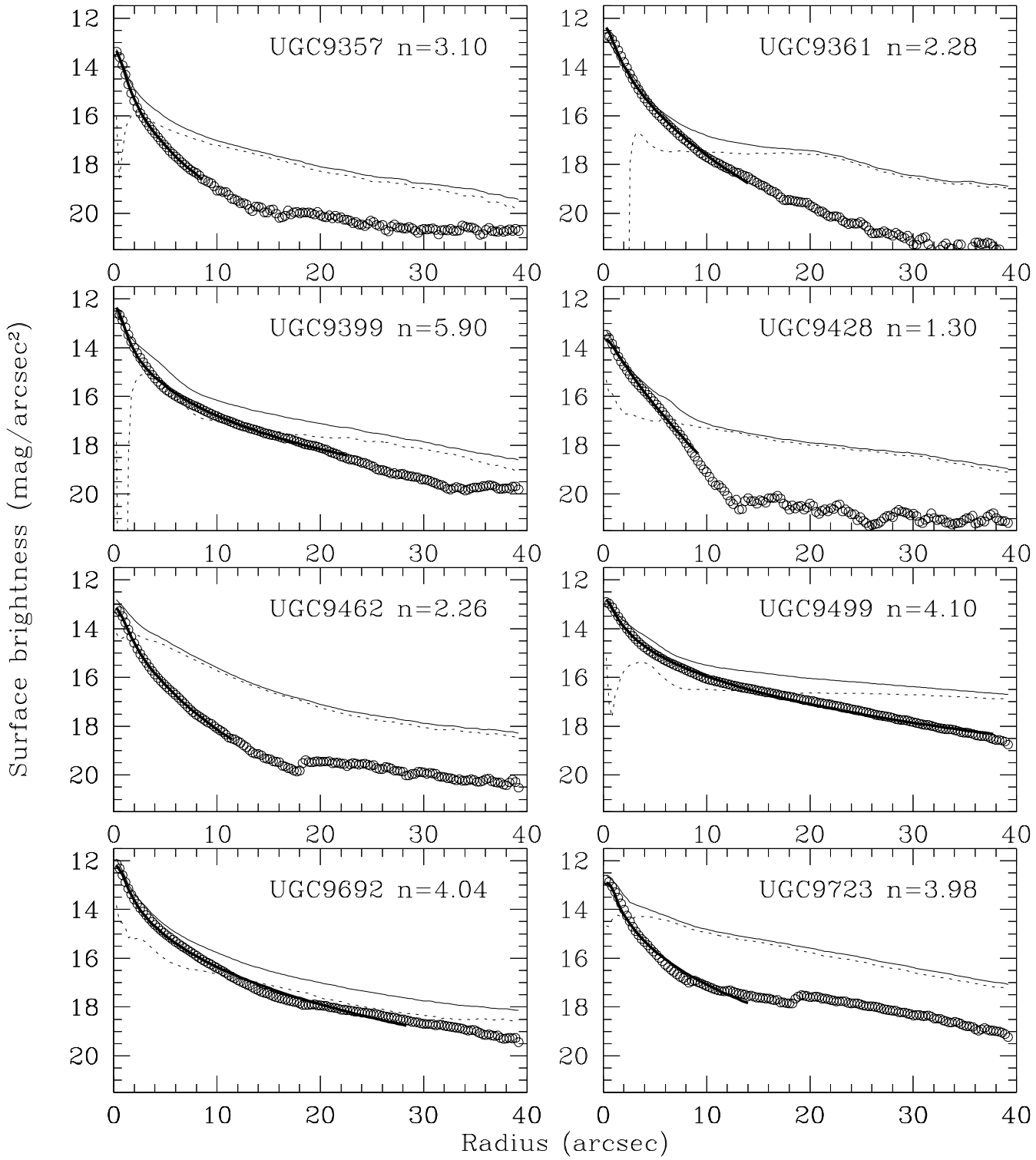

Figure 1: Continued

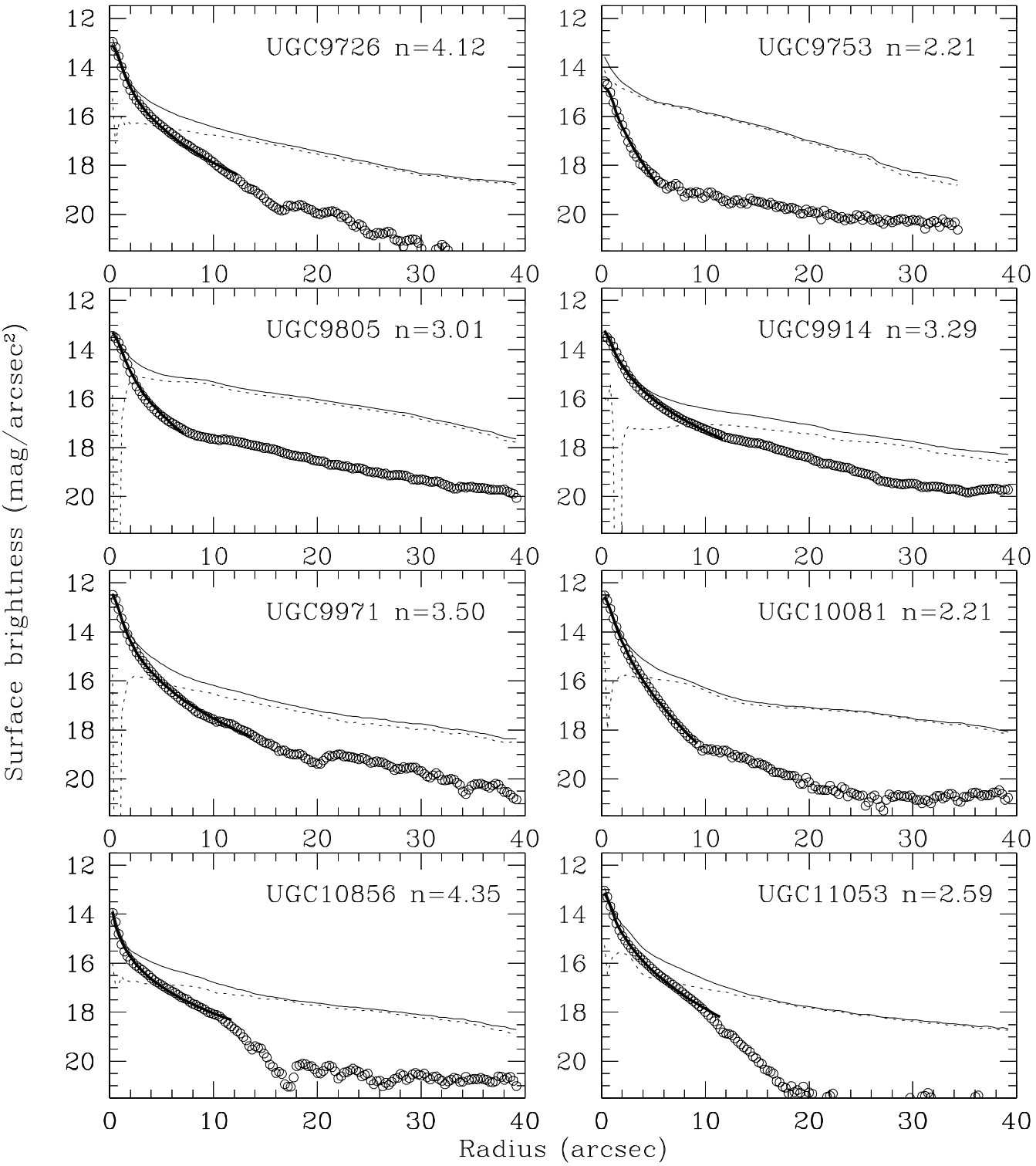

Figure 1: Continued

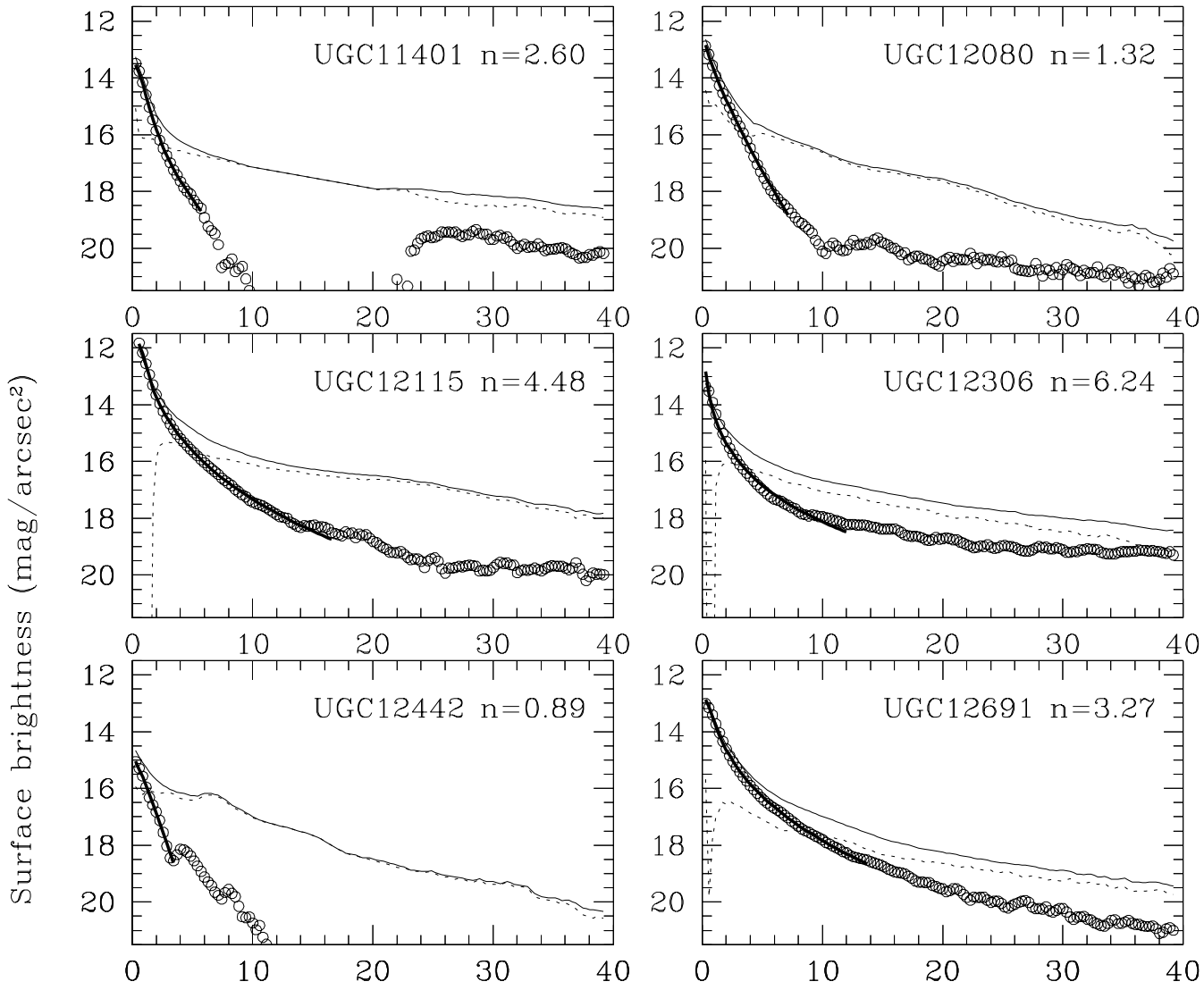

Figure 1: Continued

B PSF of the observations

Here we give the profile of the point-spread function (PSF) as measured using bright stars in the field of four of the galaxies of the sample. The Gaussian best fitting Gaussians and the corresponding full-width at half-maximum are also given. Notice the absence of any large exponential "wings" in the PSF, that would seriously affect the measured bulge profiles in the center.

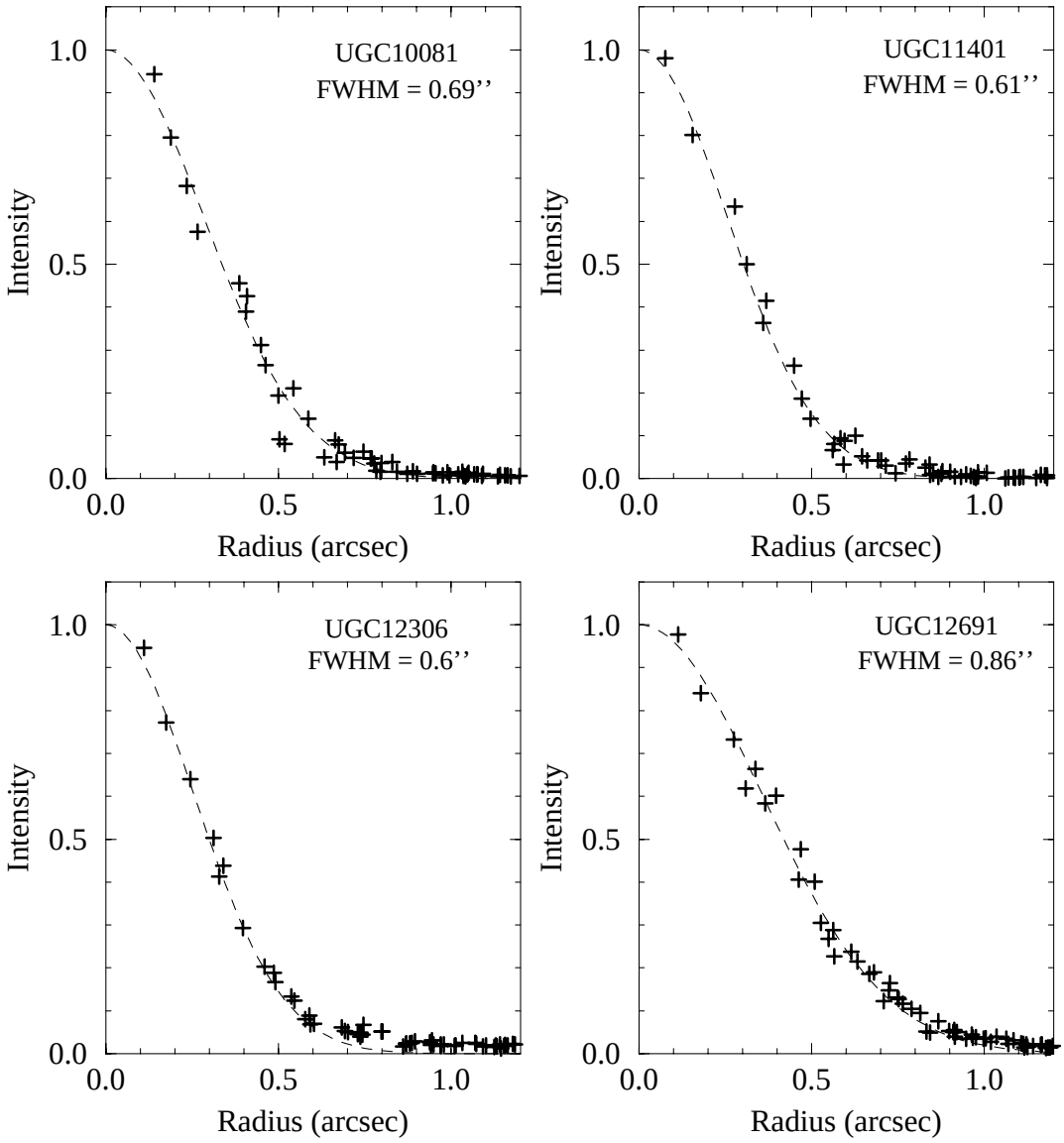

Figure 1: The PSF of the observations, measured by stellar profiles in the frames. *Dashed lines:* The best-fitting Gaussian.